UCLouvain

epl

École polytechnique de Louvain

Comparison of 3D acquisition techniques for the digital reconstruction of bowed instruments

Author: **Pauline Terlinden**
Supervisors: **François Glineur, Anne-Emmanuelle Ceulemans**
Readers: **Philémon Beghin, Paul Fisette**
Academic year 2024–2025
Master [120] in Mathematical Engineering

Abstract

In the end of the 16th century, size standards were set on bowed instruments by conservatories and to fit these new dimensions, some of the ancient instruments were reduced. It is now a hard task to quantify the impact of such a reduction on the morphology of the instruments. Having an accurate 3D numerical representation for this purpose is crucial. Nowadays multiple technologies and their implementations are available to achieve this 3D reconstruction but they differ in price and time needed. More recent and less time consuming technologies such as the optic scan and photogrammetry were compared in this work to industrial and medical computed tomography (CT) scans with a known good accuracy and reached a sub-millimetre distance with them. The iPad pro True depth and LiDAR features for mesh acquisition were also evaluated.

Acknowledgement

I would like to thank my advisors, François Glineur and Anne-Emmanuelle Ceulemans for the time they have taken for me. Their insights and help during the year were precious.

I would like to thank Philemon Beghin, PhD at UClouvain for his support, answers and the availability that he showed during this year, it was great to know that he was always nearby to provide support whenever needed.

Finally I would like to thank my mother, I hope one day I will be half the woman you are.

Contents

Chapter 1

Introduction

The violin that we see nowadays is an instrument that appeared in Italy during the second part of the 16th century. It is only 200 years later, around the middle of the 18th century, that size standards have been imposed on violins [2]. These standards can vary from country to country, meaning that for example in France and in Germany they are different. The instruments had to fit specific measurements in height, width, and shape. Some violins manufactured before the application of the standards were reduced in order to comply with the requirements. The reducing operation can consist, for example, in the removal of a central strip (Fig. 1.1) or in the removal and modification of the upper and lower curves (Fig 1.2). These figures are taken from [1].

The family of instruments concerned by the reducing is the family of ancient bowed instruments. It is formed by the present violin, viola and cello. These three instruments, although they differ by size, share a common morphology: they are divided in three parts (Fig. 1.3) : the head, the neck and the body, also called the sound box. Going further with the sound box (Fig. 1.4), the two main surfaces are the sound board and the back, connected by the ribs. As the most of the reducing consequences are visible separately on the back and on the sound board, it is sufficient to analyze each plate on their own and not the ribs. On the sound board f-holes are carved in order to propagate the sound.

FIG. 1.1 – *Removal of a central strip*

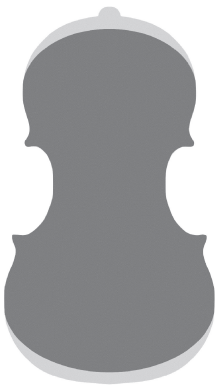

FIG. 1.2 – *Removal of upper and lower crescent*

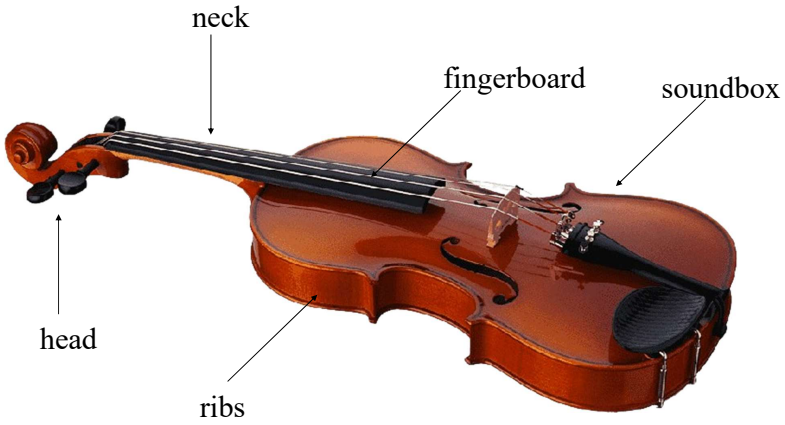

FIG. 1.3 – *Anatomy of the instrument*

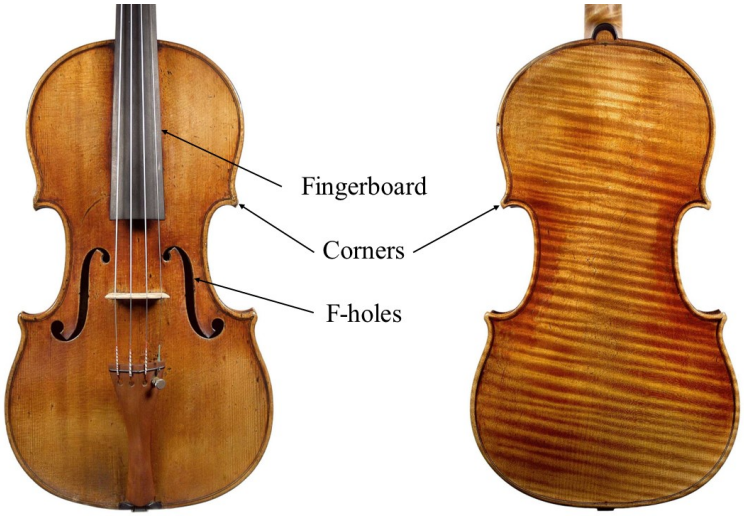

FIG. 1.4 – *View of the sound board (left) and the back (right) of a violin*

In this work, the compared entities will thus be the back and the sound board of each instrument. They are the upper and lower surface of the soundbox, that are connected by the ribs.

The identification of ancient instruments is nowadays an important task and, although an human eye can detect some reductions, it remains a subjective analysis that can sometimes fail. This is why an accurate 3D representation of these instruments could be useful. Indeed, from this representation, diverse mathematical characteristics can be extracted and have

different specificities that can help classify the instrument between reduced or not reduced. For example, along the contour of the back and the sound board, runs a 'channel of minima', it is a small, slightly recessed area, running almost along the edge of the violin, between the outer rim and the center of the plate. On Fig. 1.5, there is a visible difference between the channel of the reduced instrument that almost merges with the contour and the channel of the non-reduced instrument that is staying at a distance relatively constant to the border all around the plate.

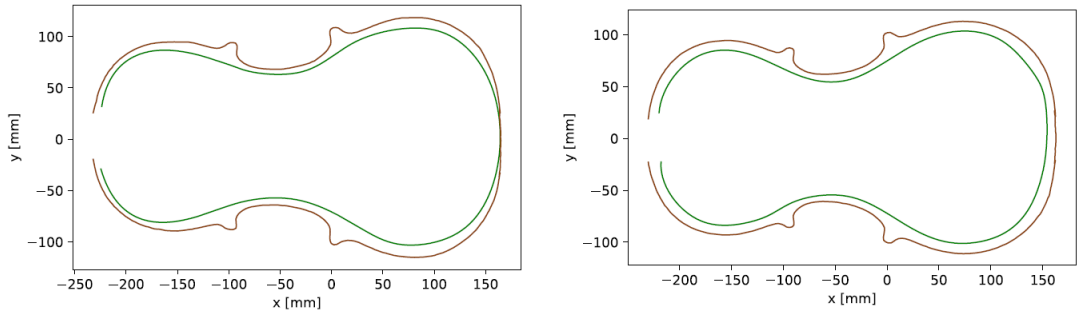

FIG. 1.5 – *Channel of minima (green) and contour (brown) of a reduced instrument (left) and not reduced instrument (right). Figures from [7]*

The 3D representation used to perform analysis such as the one described before can be produced by different acquisition techniques. Three previous works have been conducted on this specific subject at the UClouvain university, they already explored two different acquisition techniques. The first one is the photogrammetry that consists in taking multiple photographs of an object at various angles to reconstruct the object with a software. The second one is the medical computed tomography scan (CT-scan) that uses X-rays to create multiple cross-sectional images of the scanned object. In her master thesis [3], L. Motte tried to reconstruct instruments with a photogrammetric approach using a smartphone. In his master thesis [4], R. Lothaire used CT scans of the instruments for further analysis. A third master thesis [5] was conducted by P. Beghin, he returned to photogrammetry but this time with more sophisticated equipment and he could compare it with the CT scans from R. Lothaire. This photogrammetry approach is further analyzed in the context of his PhD.

This master thesis aims to compare the different acquisition techniques used in the previous works and other ones as the industrial scan, the laser scan, the optic scan and the technologies embedded on the iPad pro. After the state of the art, these technologies will be explained and the pre-processing of these output will be described. Then the measurement used in this work will be exposed and used for all of the comparison. Ultimately a more global approach will compare the error of these acquisition techniques. The instruments that will be analysed thereafter have been kindly lended by two different institutes : the Musical Instruments Museum from Brussels and the Philarmonie de Paris, Musée de la Musique.

Chapter 2

State of the art

The subject of violin reducing and digital Reconstruction has already been the focus of three previous master theses at the UClouvain. The first one was conducted by L. Motte [3], she used a photogrammetric approach with pictures taken with a basic camera in order to reconstruct the violin's shape. In her process to reconstruct the instrument, she took pictures with the violin laying horizontally on a support, to maintain the light stable she rotated the instrument. She then used the software AutoDesk recap [1] to reconstruct the two parts of the instruments. The 3D representation of the instrument was exported in RCM (ReCap Model) format that was converted in TXT for the rest of her work. She further used Matlab [2] to process the resulting 3D representation of the instruments, the computation of the channel of minima she could achieve is visible on Fig. 2.1. The results were promising but lacking of precision due to the absence of professional equipment.

The second master thesis was written by R. Lothaire [4], he decided to study the violin morphology based on medical CT-scans. The output of these scans are 2000 DICOM files (Digital Imaging and Communications in Medicine) that are grey scale images representing the cross sections of the instrument. In order to use these files for further calculations, he wrote a program to transform them into black and white pixel matrices. This would allow him to compute, for example, the channel of minima, see Fig. 2.2. The improvement between the first photogrammetry approach and the CT-scan one is clearly visible.

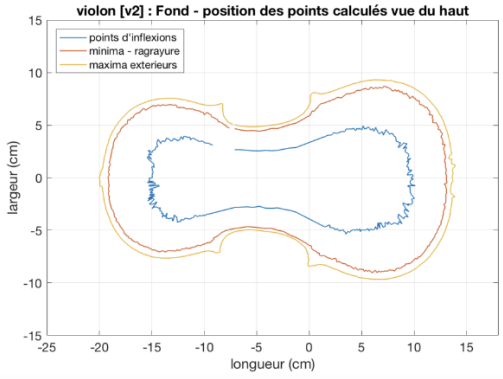

FIG. 2.1 – *Map of a violin back from [3]*

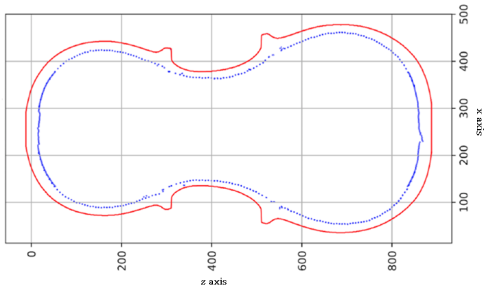

FIG. 2.2 – *Cuypers 2833 sound board channel of minima from [4]*

1. `www.autodesk.com/products/recap/overview\protect\relax\let?term=1-YEAR`
2. `www.mathworks.com/products/matlab.html`

The results obtained with the medical CT scans provided a good accuracy but this method has some important drawbacks. Indeed to scan an instrument, it needs to be taken to a hospital and the scanning process must be done when it is not required for a patient. Furthermore, to leave the museum the instruments must be insured and for the one carrying pathogens it is simply impossible. Therefore in his master thesis [5], P. Beghin decided to return to photogrammetry. He was able to organize a professional shooting with a light tent, an automatic turntable and a wooden stick to maintain the violin vertical that allowed for the complete reconstruction of the instrument. He used the Agisoft Metashape [3] professional software to reconstruct the instrument. The precision of the reconstruction is claimed to be increased by a factor 30. The instruments were exported in OBJ format and he further processed them on meshlab [4]. Then it was possible to extract the features of the instrument, such as the channel of minima shown in Fig. 2.3, in python, he worked with the PLY (Polygon File Format) format.

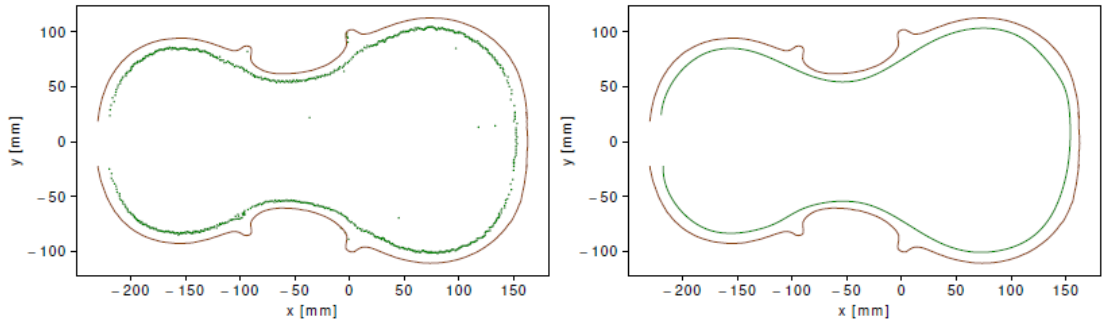

(a) *Raw minima* (b) *Channel approximation*

FIG. 2.3 – *Sound board channel Cuypers' viola from [5]*

In his work, he then compared the meshes obtained with the photogrammetry with the meshes obtained with the CT-scans. For this process either the mesh of the backs or the sound board are compared. He used a point-to-point metric to quantify the distance in millimeters between the two meshes. The way to calculate this distance is: for every point of one point cloud, a corresponding point from the other point cloud (the nearest) is identified, then the distance is calculated as the average of the Euclidean distances between these pairs. These results are summarized in an article he wrote, [7] and are the following: for the two instruments he compared, the distances were of 0.301 mm and 0.215 mm.

3. `www.agisoft.com/`
4. `www.meshlab.net`

Chapter 3

Data acquisition

This chapter aims to present the different technologies, the specifics of the measurement devices used and which instruments were scanned for each of these technologies. In total five instruments will be compared: two belong to the Philharmonie de Paris - Musée de la musique: the Andrea Amati (hereafter referred to simply as Amati) viola no. inv. 1731 and the Amati Cello inv. no. 2020 and three to the Musical Instruments Museum in Brussels: the Borbon cello inv. no. 1374, the Boussu Cello inv. no. 2863 and the Hofmans violin inv. no. 1355. They will be referenced using their inventory number [5] [6]. The different outputs of the acquisition techniques will be further analyzed in the next chapter.

3.1 Medical CT-scan

A Computed Tomography scan (CT-scan), see Fig. 3.1, is obtained as follows : a motorized source shoots beams of X-ray on the subject while rotating around it. A receptor located opposite of the subject detects X-rays as they pass through the subject and sends them to a computer. A collection of cross-sectional images is then produced by the computer. Each pixel on these 2D-slices is representing the radiosensitivity of it. The drawbacks of this technology is that it is rather difficult to have an instrument scanned by it. Indeed as the price of a medical CT scan is approximately one million euro, the solution is to go to a hospital to use one of the machine they have. The scanning session must occur when no patient needs to use it and two technicians must be there to carry on the scanning process. Moreover the instruments must be insured to leave the museum and for some of them carrying pathogens it is even impossible to scan them.

The instrument inv. no. 2863 was scanned at the Erasme hospital while the instrument inv. no. 1355 was scanned at Saint-Luc hospital in 2017 on a scanner with the following specifications :

- Device UID : 1.3.46.670589.33.1.2200303521616
- Device Name : IQON-860010
- Device Manufacturer : Philips
- Device Model Name : IQon - Spectral CT
- Device Physical Location : UCL St Luc

5. `www.carmentis.be`, for the MiM
6. `collectionsdumusee.philharmoniedeparis.fr`, for the Musée de la musique

FIG. 3.1 – *Medical CT scan*

The voltage used for the instrument 1355 was 140 kV and its current was of 244 mA. The output of both scans is a series of DICOM (Digital Imaging and Communications in Medicine) files, see Fig. 3.2. This is a format widely used in the medical community.

FIG. 3.2 – *Planar cut in DICOM (output of a medical CT scan)*

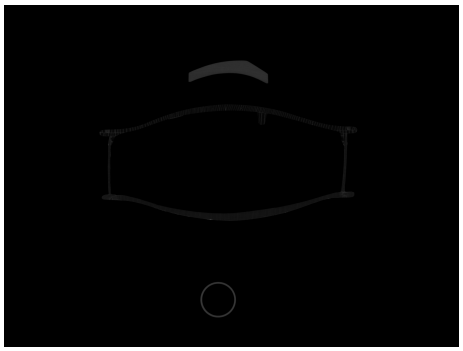

FIG. 3.3 – *Planar cut in TIFF (output of an industrial CT scan)*

3.2 Industrial CT scan

An industrial CT scan works on the same principle as a medical CT scan but while medical CT scans are designed for imaging soft tissues and bones using moderate X-ray levels safe for humans, industrial CT scans emit significantly higher radiation levels that penetrate dense materials like metals and composites. Thanks to this increased energy the resolution is finer. For the kind of machine used here, the voltage can go up to 450 kV.

FIG. 3.4 – *Industrial scan phoenix v|tome|x L 450*

The drawbacks of the industrial CT scan are similar to the ones of the medical CT scan. First, the price of an industrial CT scan lies between 200,000 and 500,000€, that is unaffordable just to scan instruments. As for the medical CT scan it is thus needed to insure the instrument, bring it to a place owning one and to scan it with the help of a technologist. The Musée de la musique in Paris had on of their instrument scanned: the Amati viola inv. no. 1731. The voltage used for this scan is 130 kV and the current is 975 mA. The specifications of the scan [7], see Fig. 3.4 that was used are :

- Device Version : 2.5.1.17206
- Device name : v|tome|x L 450
- Device Manufacturer : Baker Hughes

The output of this industrial scan are 3500 TIFF (Tagged Image File Format) files, as shown on Fig. 3.3.

3.3 Photogrammetry

Photogrammetry is the process of taking multiple pictures of an object and to create a 3D model of it. It consists in first taking pictures of the subject and the second one in creating a 3D model from the pictures. The pictures have to be taken from multiple angles and heights to cover the whole subject. They also must be overlapping for the reconstruction part to work the best, indeed in the next part, key points are detected and matched across the pictures. These pictures are usually taken with standards cameras or drones. The second part is the image processing that is usually carried out by a software. It starts by detecting the key points and aligning the pictures. Then a point cloud is build and finally a mesh consisting of vertices and edges is created. The main advantage of photogrammetry is the ease of realization as it only needs one professional camera, a setup and a few minutes per instrument to capture the images.

3.3.1 Photo acquisition

A first session of photogrammetry for some instruments took place at the Museum of Instruments (MIM) of Brussels in 2022, the complete process is the same as the one

7. www.bakerhughes.com/fr/waygate-technologies/industrial-radiography-and-ct/industrial-3d-metrology-solutions/phoenix-vtomex-l450

FIG. 3.5 – *Setup for the photogrammetry at the Musical Instruments Museum (Brussels), from [5]*

described in [5], p.17. In a nutshell the instrument was placed on an electric turntable inside of a light tent. Then photographs were taken from a static point of view while the instrument was rotating at regular angles and from different positions (lying down and standing on a wooden stick), as on Figure 3.5. This operation was carried out by a professional photograph I. Thys. The instruments from the MIM with inventory numbers 1355 and 1374 were scanned during this session.

A second session of photogrammetry for two instruments was held in Paris at the Cité de la Musique in april 2024. The conditions were slightly less optimal as no light tent nor automatic turntable was available. The first instrument is the Amati viola number 1731, it was held vertical by a metal arm on the neck skimming on a polystyren support. The pictures were then taken by J. Toupance who was turning around the instrument and capturing it at different heights.

The second instrument is the bass also from the violin maker Amati with inventory number 2020. The specificity of this bass is that its back and sound board are separated and for conservation reasons they are not gonna be put together again. The back of the instrument was simply laying on the table, as shown on Fig 3.6 . The sound board was hanging vertical held by a metallic arm and resting on a transparent plastic support, as shown on Fig 3.7.

FIG. 3.6 – *Setup for the photogrammetry at the Musée de la Musique in Paris, sound board of instrument inv. no. 2020*

FIG. 3.7 – *Setup for the photogrammetry at the Musée de la Musique in Paris, back of instrument inv. no. 2020*

3.3.2 3D reconstruction

The procedure used to obtain a 3D model from the pictures is the same for all of the instruments. To avoid negative background interference the pictures are masked, meaning that specific areas of the images are covered to focus only on the desired part (the instrument). This part could be done automatically with Photoshop [8] but still had to be double checked. Then the meshes are obtained with the software Agisoft Metashape [9]. The latter first creates a point cloud and then ultimately a 3D model that can be exported in OBJ. The parameters in Metashape were the predefined ones and the accuracy was set to high for all parts, as shown on Figures 3.8 and 3.9 from the Agisoft Metashape User Manual.

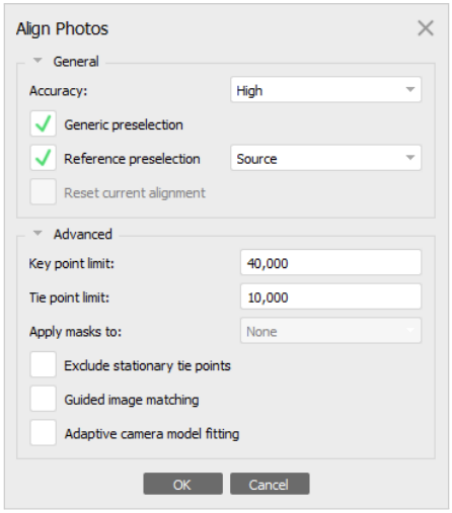

FIG. 3.8 – *Agisoft align photos dialog*

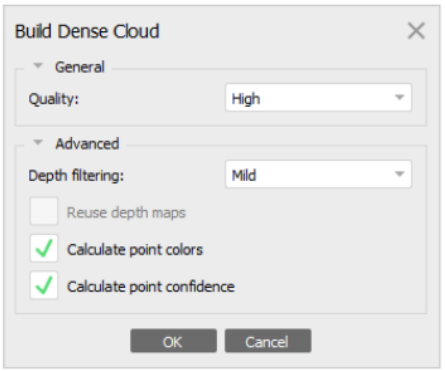

FIG. 3.9 – *Agisoft build dense cloud dialog*

3.4 Optic scan

The optic scan technology which is the subject of this research is Structured light. A device that uses Structured light technology is made up of one (or more) cameras and a projector. The projector emits a known pattern (such as stripes) that becomes distorted upon contact with the subject's surface. The camera then captures the distorted pattern (from another point of view than the projector) and from the correspondences, different depths are calculated by a triangulation technique. An optic device costs around 20,000€. The specifications and the parameters of the scan used in this work [10] are:

- Device Manufacturer : Shining 3D
- Device Model Name : EinScan HX
- Acquisition parameters
  - Source : LED
  - Acquisition Mode : Rapid
  - Precision : 0.3 mm
  - Alignment : features

8. www.photoshop.com/en
9. www.agisoft.com/
10. www.einscan.com/einscan-hx/

- Mesh parameters
  - Unwatertight
  - No filter

To reconstruct the surface, the handheld scanner must scan the object from multiple angles, the process is visible on Fig 3.10. The real-time reconstruction is performed on a computer connected to the scanner via cable, see Fig 3.11. It is a continuous process in which the person holding the scanner covers the whole surface.

FIG. 3.10 – *Optic scan acquisition*

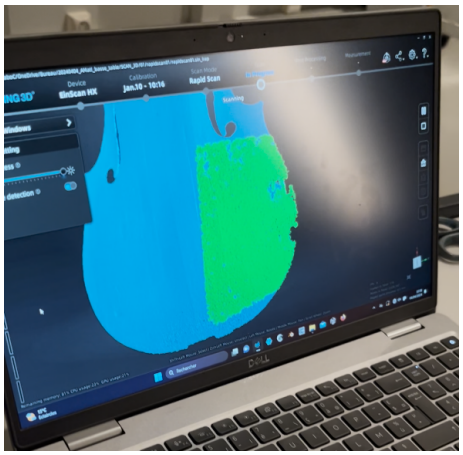

FIG. 3.11 – *Optic scan reconstruction*

The output of these scans is a PLY (Polygon File Format) file for either the sound board or the back depending on what has been scanned. Three instruments were scanned using this device: the inv. no. 1374, 1731 and 2020.

3.5 Laser scan

The device that uses laser technology on this work relies on time-of-flight. Time-of-flight lasers emit a beam in one direction and the detector measures the time taken for the beam to cover the round trip. Repeating this process in multiple directions allows to capture a whole subject. Laser scanner devices of the type that will be used cost around 80,000€. A. Peeters[11] kindly carried out the laser scanning process. The device that was used and its parameters are :

- Device Manufacturer : Topcon
- Device Model Name : GLS-2200[12]
- Scan Mode : Detailed

Three instruments were scanned with this device, all belonging to the Musical Instruments Museum: one violin (inventory number 1355), one cello (inventory number

11. Assistant in archeology at UCLouvain
12. `www.topconpositioning.com/us/en/solutions/technology/infrastructure-products/gls-2200`

2863) and one bass (inventory number 2879). The device was installed on a small table with or without an additional box to raise it from 20 cm (used for the cello). The table was approximately 2 m distant from the instrument. The setup for the violin and the bass is shown respectively on fig 3.12 and fig 3.13. The instrument inv. no. 2879 was not scanned with any other acquisition technique and will therefore not be compared but the setup used for this instrument is the same as the one used for the cello.

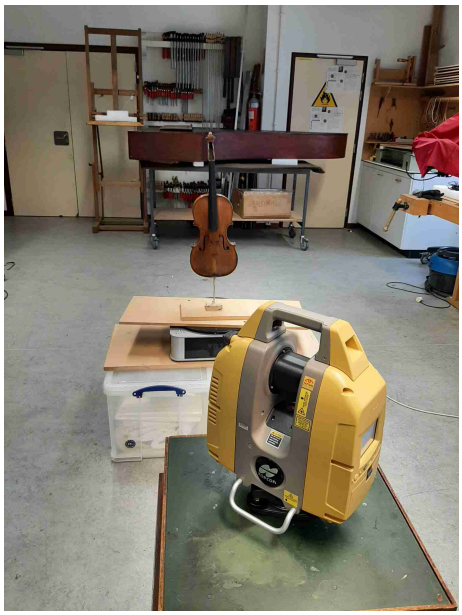

FIG. 3.12 – *Setup laser scan 2879*

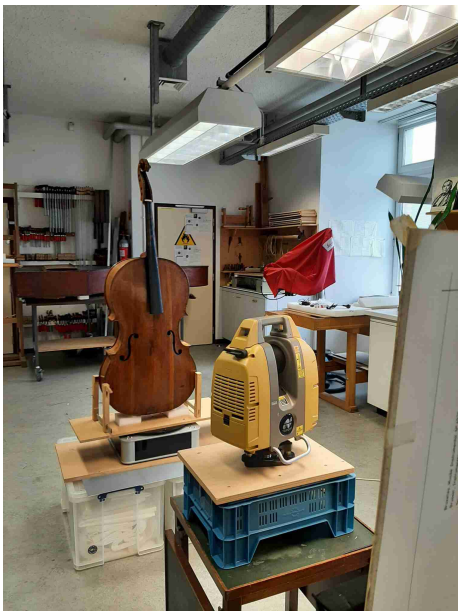

FIG. 3.13 – *Setup laser scan 2863*

For each scanned scene, the device produces a LAS (Log ASCII Standard) file that is a point cloud format.

3.6 iPad

The iPad has two different cameras, each featuring a different technology. The front camera is what Apple calls the 'True Depth Camera' and the back camera is simply called camera, equipped with a LiDAR scanner.

The LiDAR technology as implemented in the iPad uses pulses of laser light to measure the distance between the sensor and objects in the environment. By emitting thousands of laser pulses per second and calculating the time it takes for each pulse to return, LiDAR generates a precise 3D map of the surroundings, enabling accurate distance measurements up to five meters.

TrueDepth, on the other hand, is a depth-sensing system primarily used for facial recognition (Face ID). It projects over 30,000 infrared dots onto the user's face to create a detailed depth map. The infrared camera then captures this dot pattern, and algorithms process the data to create a highly accurate 3D model of the face. Unlike LiDAR, which is optimized for longer distances and environmental mapping, TrueDepth is designed for

close-range precision. The iPad that was used answers to the following characteristics:

- Model Name : iPad Pro (12.9-inch) (4th generation) [13]
- Model Number : MXAT2NF/A
- Serial Number : DMPDJ59CNR71
- iPadOS Version : 17.4.1

Different applications take advantages of these sensors to do 3D reconstruction. Two of these were tested: Scaniverse [14] and Heges [15]. The only instrument that was scanned using the iPad is the violin with inventory number 1355. It was standing on a wooden stick on a large table as pictures 3.14 and 3.15 show. For all of the applications, the user simply has to turn around the object at various heights and angles in order to scan the whole. During the scanning process, it was found that, when turning multiple times around the instrument, the surface from the second turn would not overlap with the first one creating multiple layers of the instrument. The price of an iPad Pro is around 1,000€.

FIG. 3.14 – *Setup iPad scan*

FIG. 3.15 – *Setup iPad scan*

3.7 Conclusion

In the context of this work, the comparisons for each instrument will be executed between pairs of acquisition techniques. As the instruments were scanned by a few techniques each, the list of comparisons will not be exhaustive. Table 3.1 shows an overview of the data collected, the back and the sound board (sb) are referring to the description in Fig 1.4.

13. `www.apple.com/befr/ipad-pro/`
14. `scaniverse.com`
15. `hege.sh`

	1355	1374	1731	2863	2020
CT-scan	back+sb	×	×	back+sb	×
Photogrammetry	back+sb	back+sb	back+sb	×	back+sb
Optic Scan	×	sb	back+sb	×	back+sb
Laser Scan	back+sb	×	×	back+sb	×
Industrial Scan	×	×	back+sb	×	×
iPad	back+sb	×	×	×	×

TAB. 3.1 – *Summary of acquisition techniques operated on the instruments*

Chapter 4

Preparation of the compared entities

4.1 Standardization

Each technology produces a different output representing the scanned instrument. These outputs are stored in various types of files that need to be transformed in a unique type such that a comparison is possible. This common output is the PLY file (Polygon File Format), consisting of a list of vertices composing the mesh and a list of edges between these vertices. It is a file widely used to represent meshes thus is available on a vast number of softwares and is easy to use on python as libraries exist to handle them.

The **industrial scan** ouptut were TIFF (Tagged Image File Format) files. They were uploaded in 3D slicer[16] that transforms the images in a 3D model. Then by creating a segment (a selection of a part/the totality of the 3D object) on the software it was possible to export it as a PLY file.

For the **medical scan**, the output were DICOM (Digital Imaging and Communications in Medicine) files, they were also uploaded in 3D slicer and exported as a PLY file by creating a segment.

Concerning the **photogrammetric** objects, one of them (the inv. no. 1355) had already been put in PLY for a previous work by P. Beghin. The two other instruments (inv. no. 2020 and 1731) were first expressed in OBJ (a mesh format that stores the vertices, faces, normals in ASCII) and easily converted in PLY files on MeshLab[17] that can upload OBJ files.

The **optic scans** were written in STL (a STereoLithography file contains a sucession of triangular facettes expressed with their three vertices and associated normal). This file is also handled by MeshLab and was converted into PLY on the latter.

From the LAS files realised at different angles of the instrument by the **laser scan**, only the one facing the sound board and the one facing the back were kept and handled separately. A LAS file (Light Detection and Ranging) contains a succession of 3D-coordinates that was converted in a ply file on MeshLab. The point clouds resulting from the scan showed unexpected behavior as for each point forming the back or the sound board some "noise" points are lying under it. This phenomenon is visible on Fig. 4.4.

16. `www.slicer.org` , version 5.6.1
17. `www.meshlab.net`

Two different problems were encountered with the laser scan. First, unwanted points are located inside the f-holes, probably due to the edges of the f-holes causing multiple reflections, see fig 4.2 and fig 4.1 and around the sound board, see fig 4.3, those are artefacts from the scanning method and due to the sharp angle that had to be captured. Those were manually removed on MeshLab.

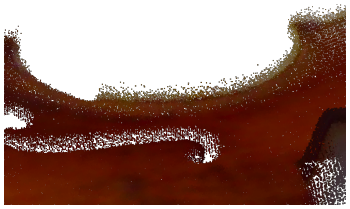

FIG. 4.1 – *2863 Noise on top of sound board*

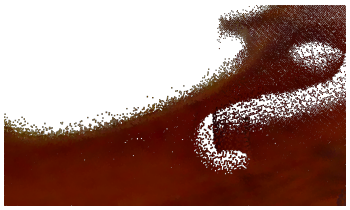

FIG. 4.2 – *2863 Noise underneath of sound board*

FIG. 4.3 – *2863 zoom on f-holes*

The second problem that has arisen is that after aligning the sound board (or back) of the instrument with the axis as specified in the introduction, multiple points are to be found along the z axis, it seems that the laser scan produced a regular grid of 1x1x1mm with at some locations 4 points in the $z-$direction, see fig 4.4. The reason for such a noisy result is probably due to an interaction between the laser beam and the surface of the instrument and its varnish.

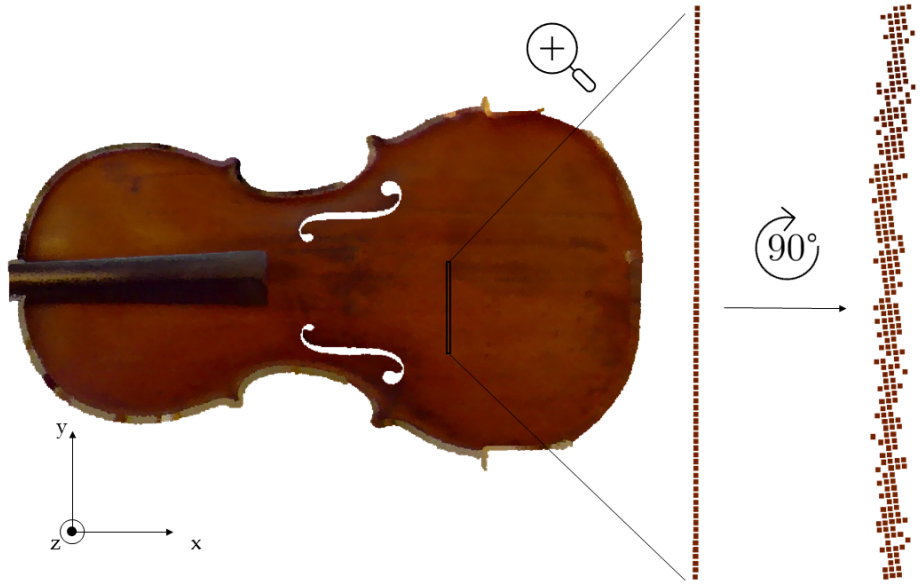

FIG. 4.4 – *Visualization of grid by laser mesh*

The solution to this problem was to align the mesh on MeshLab in order to produce "stacks" of points and try to have (almost) the same z-coordinate. This way a simple program on python could create a grid of 1mm x 1mm and keep only the point with the maximal value in z. The downside of this program is that since the sound board is not exactly planar, some point are left out as they fall on the same case. Despite this issue it works quite nice and only a few points are missed which shouldn't alter the mean result of

the comparison.

The last acquisition technique is the **iPad**. The two applications used for scanning (Scaniverse and Heges) allowed to export the meshes in the PLY format therefore no further step is necessary.

4.2 Pre-processing

As some of the acquisition techniques scanned separately the back and the sound board and the back of the instrument, the compared entities will be these two parts. Thus from each PLY file, a general procedure is followed. First the back and the sound board are separated and saved as two different files. Then a first manual approximate removal of faces is done along the border. For the sound board, more work has to be done, the f-holes and the area under the fingerboard need to be removed, as on Fig.4.5.

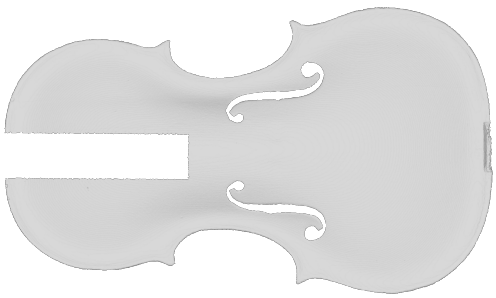

FIG. 4.5 – *Sound board of a violin*

The mesh has then to be aligned such that the $x-$axis crosses the length of the board with the largest part of the back/sound board aligned in the positive direction, the $y-$axis is aligned with the two left corners and the back/sound board has its visible part visible from the top of the $z-$axis (see Fig 4.6). The alignment to the axes is performed with PCA (principal components analysis) and rotated by 90° steps to fit the desired orientation.

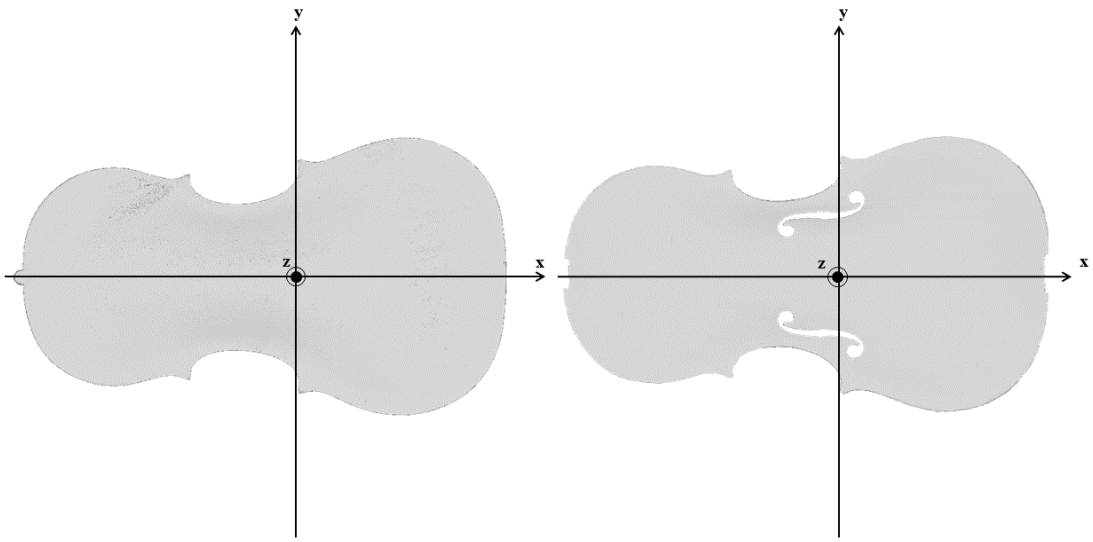

FIG. 4.6 – *3D axis*

Next follows a delineation process established in [5], the code written for this purpose intends to "delineate a contour on a violin sound board or back mesh. More precisely, it preserves the upper part of the sound board or back, i.e., it removes the "vertical" parts that exceed from the "strict" contour and that constitute the ribs.", see Fig. 4.7 and 4.8. The code is designed to work for the specific alignment described previously.

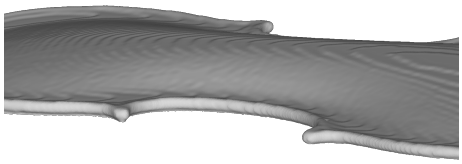

FIG. 4.7 – *Instrument before delineation process*

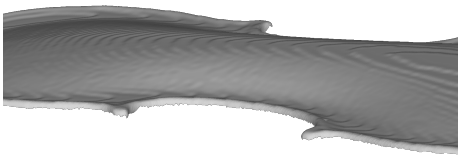

FIG. 4.8 – *Instrument after delineation process*

Ultimately the number of vertices can be reduced by using the function $simplification$: $QuadricEdgeCollapseDecimation$ from MeshLab, that simplifies 3D models by merging vertices while minimizing geometric distortion. It uses a quadric error metric, represented by a quadratic matrix for each vertex, which quantifies the geometric error introduced by collapsing two vertices. The algorithm selects the collapse that minimizes the total error [9]. The number of 100,000 vertices is chosen for the majority of the meshes because it was found to be a good trade off between the computational speed and the accuracy in [7].

Chapter 5

Point Cloud Distances, Registration

5.1 Point cloud distances

As the main objective of this work is to compute the distance between different meshes, such a measure must be defined. Two possible distances are described in [7]. Considering two point clouds denoted $s = \{s_i\}_{i\in\{1,\dots,N_s\}}$ and $p = \{p_i\}_{i\in\{1,\dots,N_p\}}$ with respectively N_s and N_p points, the first distance is the 'point-to-point distance' :

$$D(s,p) = \frac{1}{N_s}\sum_{i=1}^{N_s}\left\|\boldsymbol{s_i} - \boldsymbol{p_{nn(i)}}\right\| \tag{5.1}$$

where

$$p_{nn(i)} = \arg\min_{p_j\in p}\left\|s_i - \boldsymbol{p}_j\right\|. \tag{5.2}$$

Thus, for each vertex $\boldsymbol{s_i} \in \mathbb{R}^3$, the nearest neighbor $\boldsymbol{p_{nn(i)}}$ is identified from the set p. The distance between each vertex $\boldsymbol{s_i}$ and its nearest neighbor $\boldsymbol{p_{nn(i)}}$ is computed, and these distances are averaged over all vertices in s to determine the average distance between the two point clouds. This distance is not symmetric as the closest neighbor of a point in s does most probably not have the point in s as closest neighbor due to the huge number of points in the meshes.

The second distance is computed using the normal n_i at the point $\boldsymbol{s_i}$ and projecting the local distance onto it, it is referred to as the 'point-to-plane' distance :

$$D^2_{\text{plane}}(s,p) = \frac{1}{N_s}\sum_{i=1}^{N_s}\left|\left(s_i - \boldsymbol{p}_{\text{nn(i)}}\right)^T \cdot \boldsymbol{n_i}\right|^2 \tag{5.3}$$

The computation of the normals at each point n_i is evaluated by using the PCA (principal component analysis) of the covariance matrix of a chosen number of nearest neighbors at the evaluated point, this method is taken from [8]. In this work, the number of neighbors is always 10. This distance is a squared distance, the unit are in mm^2 such that it is a convex function that allows it to be optimized (to find its minimum) with efficient methods. The difference between these two distances is shown on fig 5.1. The 'point-to-plane' distance is the most adequate in this work as the meshes representing the instruments have different point densities and the use of the normals allows to have smaller distances for points who are falling in the middle of a face but whose nearest neighbor is more far away.

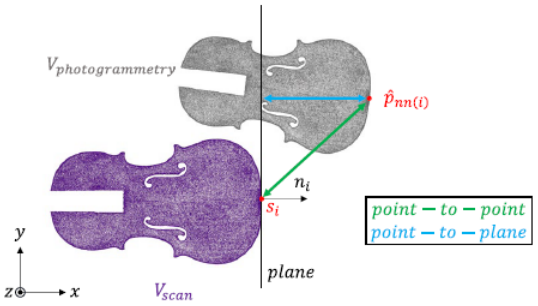

FIG. 5.1 – *Comparison between point-to-point and point-to-plane approaches from [7]*

5.2 Registration

Registration is the process of aligning two point clouds, meshes or surfaces. One mesh is fixed, its coordinates will not be changed through the process. The other mesh is moving and its coordinates are changing to match the fixed mesh. The alignment is identified by optimizing rigid parameters ($\mathbf{X} \in \mathbb{R}^3$, for the translation and $\boldsymbol{\theta} \in \mathbb{R}^3$, for the rotation) or non-rigid parameters ($K \in \mathbb{R}$, for the scaling) to minimize a chosen distance. To apply the transformation to every vertex of the moving mesh, the following formula is used:

$$\hat{\boldsymbol{p}}_{\boldsymbol{j}} = K(\boldsymbol{R}_{\boldsymbol{\theta}}\boldsymbol{p}_{\boldsymbol{j}} + \mathbf{X}) \tag{5.4}$$

where $\hat{\boldsymbol{p}}_{\boldsymbol{j}}$ is the new coordinate of the vertex $\boldsymbol{p}_{\boldsymbol{j}}$ belonging to the moving point cloud and the rotation matrix R_θ is :

$$\boldsymbol{R}_{\boldsymbol{\theta}} = \begin{pmatrix} \cos\theta_3 & \sin\theta_3 & 0 \\ -\sin\theta_3 & \cos\theta_3 & 0 \\ 0 & 0 & 1 \end{pmatrix} \begin{pmatrix} \cos\theta_2 & 0 & -\sin\theta_2 \\ 0 & 1 & 0 \\ \sin\theta_2 & 0 & \cos\theta_2 \end{pmatrix} \begin{pmatrix} 1 & 0 & 0 \\ 0 & \cos\theta_1 & \sin\theta_1 \\ 0 & -\sin\theta_1 & \cos\theta_1 \end{pmatrix} \tag{5.5}$$

5.2.1 Iterative Closest Point

The first registration method is the Iterative Closest Point (ICP) algorithm [18], whose framework is:

1. **Selection** : A subset of points is selected within the fixed point cloud. The nonselected points won't be considered in the distance to be optimized.
2. **Matching** : The nearest neighbor of all the selected fixed points are searched for in the moving point cloud.
3. **Rejection** : Outliers are rejected based on different criteria.
4. **Minimization** : Optimization is performed to minimize the distance between the corresponding points
5. **Transformation** : The moving point cloud is transformed using the estimated parameters.

A version of ICP, *simple_icp*, is implemented on python and is available on GitHub [19]. In this implementation, described in [8], the subset of selected points (whose number is defined

18. en.wikipedia.org/wiki/Iterative_closest_point
19. github.com/pglira/simpleICP

by the user) is computed in the beginning and remains unchanged. The points are selected at evenly spaced intervals across the indices. These points are then matched to their closest points in the moving point cloud. Then follows the rejection part, in the implementation two criteria are checked: the planarity of the points, that is computed as the ratio $(\lambda_2 - \lambda_3)/\lambda_1$ (where the λ_i are the eigenvalues of the covariance matrix of a chosen number of nearest neighbors, $\lambda_1 < \lambda_2 < \lambda_3$), must be greater than the threshold $min\_planarity$ (by default this value is 0.3). To satisfy the second criterion, the distances that are outside the interval $\widetilde{d} \pm 3\sigma_{mad}$ are rejected where $\sigma_{mad} = 1.4826 \cdot$ mad, mad $=$ median$_i(|d_i - \text{median}_j(d_j)|)$ and d_i are the point-to-plane distances. Finally, the minimization part is performed with respect to the point-to-plane distance described previously.

5.2.2 Full Registration

The second algorithm, used under the name of 'Full Registration' here, comes from [7]. In this article, one implementation of registration is effectuated and is quickly described here. There is no selection nor rejection process and all of the points from the fixed point cloud are kept through the whole process. The matching stage is executed with one of the two distance metric described, the point-to-point or the point-to-plane. Finally, the minimization part is performed using the Powell method using the existing Python implementation *scipy.optimize.fmin_powell*. In this method, a scaling factor can be optimized as well, making it possible for a mesh to be enlarged or shrunk such that the distance is further minimized.

The programming language used in this work is Python whose main advantages are that it is free, has lots of packages and is widely spread. Furthermore, some algorithms and visualization methods were already implemented by P. Beghin in this language and will be used, such as the delineation function.

Chapter 6

Comparisons

In this chapter, all of the comparisons are performed. Each instrument was scanned by different acquisition techniques and was thereafter pre-processed. For each pair of technique, there are two comparisons because the distance used is not symmetrical. The distance used for all of the comparison is the point-to-plane distance :

$$D^2_{\text{plane}}\,(s,p) = \frac{1}{N_s}\sum_{i=1}^{N_s}\left|\Big(s_i - \boldsymbol{p}_{\text{nn(i)}}\Big)^T \cdot \boldsymbol{n_i}\right|^2 \tag{6.1}$$

This distance is minimized in order to have the two compared plates (back or sound board) aligned. The choice of this metric and not the point-to-point is justified in this work because the meshes representing the instruments have different point densities and the use of the normals allows to have smaller distances for points who are falling in the middle of a face but whose nearest neighbor is more far away. After having optimized the distance in mm^2, the square root of the squared distances (for each point) is taken and averaged to have the units in mm that are easier to interpret.

$$D_{\text{plane}}\,(s,p) = \frac{1}{N_s}\sum_{i=1}^{N_s}\sqrt{\left|\Big(s_i - \boldsymbol{p}_{\text{nn(i)}}\Big)^T \cdot \boldsymbol{n_i}\right|^2} \tag{6.2}$$

6.1 Amati Viola 1731

The first instrument is a viola with inventory number 1731 [20] and comes from the collection of the Musée de la Musique in Paris, see Figures 6.1 and 6.2. This instrument was manufactured by Andrea Amati before 1568 in Cremone, Italy. It was originally a tenor violin and has undergone at least two transformations in its history. It has been reduced in width by removing a central strip and shortened by altering the upper and lower curves. A shield whose arms are identified as those from the royal couple, Philip II of Spain and Elizabeth of Valois is painted at the center of the back of the instrument. For this instrument, the following acquisition techniques will be compared: an industrial (318.796 vertices for the back and 281.239 for the sound board) and optic scan (97.026 vertices for the back and 95.324 for the sound board) and photogrammetry (77.666 vertices for the back and 193.791 for the sound board).

20. collectionsdumusee.philharmoniedeparis.fr/collectionsdumusee/doc/MUSEE/0157875/tenor-de-violon-recoupe-en-alto

FIG. 6.1 – *Amati Viola, front. Photo : Jean-Claude Billing*

FIG. 6.2 – *Amati Viola, back. Photo : Jean-Claude Billing*

The next table displays the optimum point-to-plane distance in mm^2 for the backs of the instrument. Each cell represents one comparison where the fixed mesh is the one of the row and the moving mesh is the one of the column. The three values are the one obtained respectively with the Iterative Closest Point method (ICP), the full registration without scaling (FR) and the full registration with scaling (FRS). The scaling factor, K, is also indicated for the scaled full registration.

Ref mesh (↓)	Photogrammetry	Optic scan	Industrial scan
Photogrammetry	×	0.0050 (ICP) 0.0049 (FR) 0.0037 (FRS K=0.997)	0.0063 (ICP) 0.0062 (FR) 0.0059 (FRS K=0.999)
Optic scan	0.0063 (ICP) 0.0062 (FR) 0.0041 (FRS K=1.004)	×	0.0108 (ICP) 0.0103 (FR) 0.0090 (FRS K=1.002)
Industrial scan	0.0080 (ICP) 0.0079 (FR) 0.0079 (FRS K=1.002)	0.0105 (ICP) 0.0102 (FR) 0.0098 (FRS K=0.999)	×

TAB. 6.1 – *Point-to-plane distances back 1731 (mm^2)*

The different trends among the three methods are visible in this table: the ICP method produces systematically the worst value of the three but is (for this table) never more than 0.0005 mm^2 from the value obtained with the second method, that is the full registration. The addition of the scaling factor improves furthermore the mean squared point-to-plane distance up to 0.002 mm^2. There is thus a significant improvement with the scaling factor.

The scaling factors are consistent for each pair, meaning that their product is close to 1. For example the comparisons between the photogrammetric and the optic scan are yielding for, either an enlargement of the photogrammetric scan by 0.4%, either a shrinking of the optic scan by 0.3% for them to match the other mesh. The photogrammetric scan is thus smaller than the optic one. The industrial and the optic scan have each an 0.1% change, indicating that they are close to having the same dimensions.

In order to get a better idea of the distances, the average of the square root of the distances for each point in the mesh is calculated such that the obtained units are millimeters. As the scaling factor induces the best value, it is the one selected for the summary.

Ref mesh (↓)	Photogrammetric scan	Optic scan	Industrial scan
Photogrammetric scan	×	0.0409	0.0566
Optic scan	0.0436	×	0.0686
Industrial scan	0.0629	0.0701	×

TAB. 6.2 – *Point to plane distances back 1731 with scaling (mm)*

The distance are fairly symmetric for each pair of technology. The pair with the lowest values is the photogrammetric-optic one with a mean of 0.0422 mm, the largest values appear in the industrial-optic pair with values around 0.069 mm.

The next table shows the results for the sound board.

Ref mesh (↓)	Photogrammetric scan	Optic scan	Industrial scan
Photogrammetric scan	×	0.0057 (ICP) 0.0053 (FR) 0.0040 (FRS K=0.997)	0.0076 (ICP) 0.0072 (FR) 0.0057 (FRS K=0.997)
Optic scan	0.0067 (ICP) 0.0064 (FR) 0.0041 (FRS K=1.004)	×	0.0062 (ICP) 0.0062 (FR) 0.0062 (FRS K=1.001)
Industrial scan	0.0069 (ICP) 0.0066 (FR) 0.0053 (FRS K=1.002)	0.0051 (ICP) 0.0050 (FR) 0.0050 (FRS K=1.002)	×

TAB. 6.3 – *Point-to-plane distances sound board 1731 (mm^2)*

The same conclusion as for the back are raised by these results for the difference between the optimization methods. The ICP and full registration method without scaling are a few mm^2 away from each other and the scaling improves further the distance. The comparison between the industrial and the optic scan is remarkable in the sense that the three methods almost give the same values, indicating that almost no scaling is needed. The other scaling factors are consistent with the ones for the backs, with the exception of the comparison between the industrial scan (reference) and the optic scan (moving) that asks for a factor of 1.002, where this factor is almost 1 (and greater than 1) for the other way around meaning that both meshes should be enlarged to fit the other one. But as the values for this comparison are really close to 1 it is not raising concern. The mean root squared distances are given in Tab. 6.4.

Ref mesh (↓)	Photogrammetric scan	Optic scan	Industrial scan
Photogrammetric scan	×	0.0418	0.0548
Optic scan	0.0410	×	0.0539
Industrial scan	0.0523	0.0481	×

TAB. 6.4 – *Distances sound board 1731 with scaling (mm)*

The values of this table lie in a small interval, they all fall between 0.0410 and 0.0548 mm. There is a quasi perfect symmetry between the optic and the photogrammetric scan, the pair photogrammetric and industrial scan also has a good symmetry. The last pair also has a certain symmetry but less remarkable.

In order to evaluate the impact of each acquisition technique for this instrument on the error, a simple model is used :

$$d_{tech_1 tech_2} = e_{tech_1} + e_{tech_2}$$

The distance for each combination is estimated as the mean of the values for the back and the sound board and for each way around (reference/moving). For example the distance between the photogrammetric mesh and the optic mesh appears four times, two times for the backs (0.0436 and 0.0409 mm) and two times for the sound boards (0.0410 and 0.0418 mm), the mean of these four values is 0.0418 mm. This value is used as an approximation of the sum of the errors for the photogrammetry and the optic scan. The following system is the result for the Amati 1731 instrument (phot = photogrammetry, opt = optic scan, indu = industrial scan) :

$$\begin{cases} e_{phot} + e_{opt} = 0.0418 \\ e_{phot} + e_{indu} = 0.0567 \\ e_{opt} + e_{indu} = 0.0602 \end{cases}$$

The errors for each method according to this system are : 0.01915, 0.02265 and 0.03755 mm for the photogrammetric, optic and industrial scan respectively. The values are the same as the one that would be obtained if computed separately for the back or the sound board and averaged. According to these values, the industrial scan is responsible for most of the distances where the photogrammetry is the least accountable.

6.2 Hofmans Violin 1355

The instrument with inventory number 1355 [21]

belongs to the Musical Instruments Museum in Brussels, shown on Figures 6.3 and 6.4. It is a violin and was manufactured by M. Hofmans in Antwerp before 1672. For this instrument, a photogrammetry (78.892 vertices for the back and 76.606 for the sound board) a medical (235.836 vertices for the back and 222.259 for the sound board), a laser (54.443 vertices for the back and 45.602 for the sound board) and an iPad scan session

21. www.carmentis.be:443/eMP/eMuseumPlus?service=ExternalInterface&module=collection&objectId=109427&viewType=

were carried out. The iPad is compared separately than the other acquisition techniques because the meshes are visually already a bad 3D representation of the instrument.

FIG. 6.3 – *Front of the violin 1355*

FIG. 6.4 – *Side of the violin 1355*

For the instrument inv. no. 1355 only the tables with the mean root squared distance are displayed (tables 6.5 and 6.6), the metric is still the point to plane one and the values are the ones obtained with the scaling factor and the full registration optimization:

Ref mesh (↓)	Photogrammetric scan	Laser scan	Medical scan
Photogrammetric scan	×	0.3230	0.3893
Laser scan	0.4871	×	0.6047
Medical scan	0.3895	0.3779	×

TAB. 6.5 – *Point to plane distances back 1355 with scaling (mm)*

Ref mesh (↓)	Photogrammetric scan	Laser scan	Medical scan
Photogrammetric scan	×	0.3736	0.3833
Laser scan	0.5135	×	0.6013
Medical scan	0.3787	0.4314	×

TAB. 6.6 – *Point to plane distances sound board 1355 with scaling (mm)*

As the scaling factors for all of the comparisons between the photogrammetric and the medical scan are arising for a change of 0.1% or less, it is reasonable to think that they have the same dimensions. The laser scans on the other hand needs to be slightly enlarged

to fit both the medical and the photogrammetric scan. In general the distances are way larger than the ones obtained for the previous instrument.

The largest values of both tables are on the line where the laser scan is the reference mesh. One explanation is that the irregularity of the mesh produces normals, see Fig. 6.5, that are not always perfectly perpendicular (in comparison, the normals of the medical scan are visible on Fig. 6.6). This makes the tables 6.5 and 6.6 rather asymmetrical except for the pair photogrammetric-medical scan. Each comparison produces about the same result for the back and for the sound board.

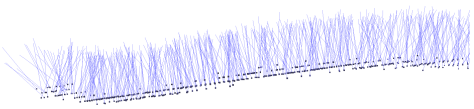

FIG. 6.5 – *Normals of a slice of the laser scan (instrument inv. no. 1355)*

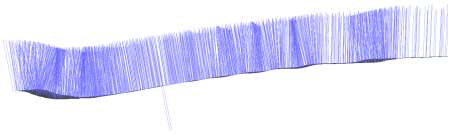

FIG. 6.6 – *Normals of a slice of the medical CT scan (instrument inv. no. 1355)*

The same exercise as computed for the Amati 1731 produces new estimations of the errors of the three technologies compared here. The equations are the following (phot = photogrammetry, las = laser scan, med = medical scan):

$$\begin{cases} e_{phot} + e_{las} = 0.4243 \\ e_{phot} + e_{med} = 0.3852 \\ e_{las} + e_{med} = 0.5038 \end{cases}$$

The errors computed are: 0.1529, 0.2715, 0.2324 mm respectively for the photogrammetric, the laser and the medical scan. Comparing the error for the photogrammetric approach of the two instruments, for the Amati it was 0.01915 mm where it rose up to 0.1529 here. It is thus eight times bigger. In general the values obtained for the Hofmans are way bigger.

For the iPad, a few tries for each acquisition technique (the LiDAR used in the applications Scaniverse and Heges and True Depth used in Heges) were effectuated but the Table 6.7 only shows the best distance that could be achieved with the scans.

iPad mesh (↓)	plate	# vertices	Medical CT scan	Photogrammetry
Scaniverse LiDAR	back	8.335	0.6118 (K=1.0227)	0.3693 (K=1.0198)
Heges LiDAR	back	74.588	1.6735 (K=1.0016)	1.5294 (K=1.0055)
Heges True Depth	back	62.227	0.5056 (K=0.9991)	0.1273 (K=0.9974)
Scaniverse LiDAR	sound board	10.572	0.8682 (K=1.0032)	0.8424 (K=1.0007)
Heges LiDAR	sound board	67.753	0.5197 (K=1.0140)	0.1972 (K=1.0119)
Heges True Depth	sound board	56.670	0.5516 (K=1.0084)	0.1860 (K=1.0099)

TAB. 6.7 – *Point-to-plane distances iPad acquisition 1355 (mm)*

The first noticeable element from the table is the difference between the medical CT scan and the photogrammetry. Indeed the latter systematically produces a distance smaller than the first with sometimes an improvement by a factor of three. The scaling factors are all yielding for an enlargement of the iPad acquired mesh only for one exception, the Heges True Depth back that slightly needs to be shrunk. Altogether the values of the distance are comparable to the ones obtained for the comparisons between the photogrammetry, laser and medical scan. There is only one value that is 1 mm higher than the other one and it it the back of the Heges LiDAR scan, that was already of a poor quality visually. In conclusion, these results are encouraging as some of them reach a distance of 0.2 mm to the photogrammetry.

6.3 Amati Cello 2020

The instrument with inventory number E.2020.1.1 [22] at the Musée de la Musique was manufactured by Andrea Amati in Italy in 1572, see Fig 6.7 and 6.8. Originally a bass violin, it was reduced at the end of the XVIIe or beginning of the XVIIIe century to become a cello. For this instrument, data has been collected with an optic scan (93.718 vertices for the back and 99.904 for the sound board) and with photogrammetry (100.585 vertices for the back and 101.083 for the sound board).

22. collectionsdumusee.philharmoniedeparis.fr/1115940-basse-de-violon-recoupee-en-violoncelle-andrea-i-amat aspx

FIG. 6.7 – *Amati Cello, photo by Claude Germain, photograph*

FIG. 6.8 – *Amati Cello, photo by Jan Röhrmann, photograph*

For this instrument, the scaling factors are all close to the value of 1, leading to the conclusion that they have almost the same dimensions (both for the back and the sound board). The values are also symmetric between the two comparisons but the results for the back are five times larger than the ones obtained for the sound board (in mm). The explanation is hard to find. The next two tables are summarizing the obtained values with the scaling factor.

Ref mesh (↓)	Photogrammetric scan	Optic scan
Photogrammetric scan	×	0.2406
Optic scan	0.2526	×

TAB. 6.8 – *Distances back 2020 with scaling (mm)*

Ref mesh (↓)	Photogrammetric scan	Optic scan
Photogrammetric scan	×	0.0790
Optic scan	0.0737	×

TAB. 6.9 – *Distances sound board 2020 with scaling (mm)*

6.4 Borbon Cello 1374

This instrument[23] belongs to the Museum of Instruments in Brussels and is a cello that was manufactured by Gaspar Borbon, see Figures 6.9 and 6.10. It was produced in

23. www.carmentis.be:443/eMP/eMuseumPlus?service=ExternalInterface&module=collection&objectId=109450&viewType=

Brussels before 1688. Only the sound board of this instrument underwent an optic scan (252.861 vertices), and the photogrammetry (81.038 vertices).

FIG. 6.9 – *Front of the cello 1374*

FIG. 6.10 – *Side of the cello 1374*

For this instrument, only the sound board was scanned, the results for the distances are shown on table 6.10.

Ref mesh (↓)	Photogrammetric scan	Optic scan
Photogrammetric scan	×	0.0213
Optic scan	0.0310	×

TAB. 6.10 – *Distances sound board 1374 with scaling (mm)*

For this set of acquisition the optic scan has to be reduced in order to fit the photogrammetric one. This scaling factor allows an improvement of 40% of the initial mean squared distance computed without scaling factor. The comparison with optic scan as a reference (0.0310) leads to a slightly higher value than the other one (0.0213) with a difference of 0.01 mm. This can be explained by the estimation of the normals at the border of the optic scan that are not perfectly perpendicular to the mesh.

6.5 Boussu Cello 2863

The cello with inventory number 2863[24] at the Museum of Instruments was manufactured by Benoît Joseph Boussu in 1752, see Figures 6.11 and 6.12. For the instrument a medical scan (102.485 vertices for the back and 95.792 for the sound board) and a laser

24. www.carmentis.be:443/eMP/eMuseumPlus?service=ExternalInterface&module=collection&objectId=109956&viewType=

scan (233.122 vertices for the back and 208.906 for the sound board) were performed. The results for the back are shown on table 6.11 and the ones for the sound board on 6.12.

FIG. 6.11 – *Front of the cello 2863*

FIG. 6.12 – *Side of the cello 2863*

Ref mesh (↓)	Laser scan	Medical scan
Laser scan	×	0.8134
Medical scan	0.6925	×

TAB. 6.11 – *Distances back 2863 with scaling (mm)*

Ref mesh (↓)	Laser scan	Medical scan
Laser scan	×	0.9176
Medical scan	1.0145	×

TAB. 6.12 – *Distances sound board 2863 with scaling (mm)*

For the comparisons between the backs, both of them are demanding an enlargement of the scan for it to fit the other one. The fitting is visually not concluding and the laser point cloud is slightly rotated from the medical mesh. This is probably due to the irregularity of the laser scan and the bad evaluation of the normals (comparable to the ones shown on Fig. 6.5) that follows.

Chapter 7

Global comparison

The next image gives a global overview of all the mean root squared point-to-plane with the scaling factor distances derived from the prior chapter. A line between two acquisition techniques means that an instrument was scanned with both techniques making it possible to calculate their distance. For each pair, each technology is alternately the reference and the moving mesh (sb stands for sound board).

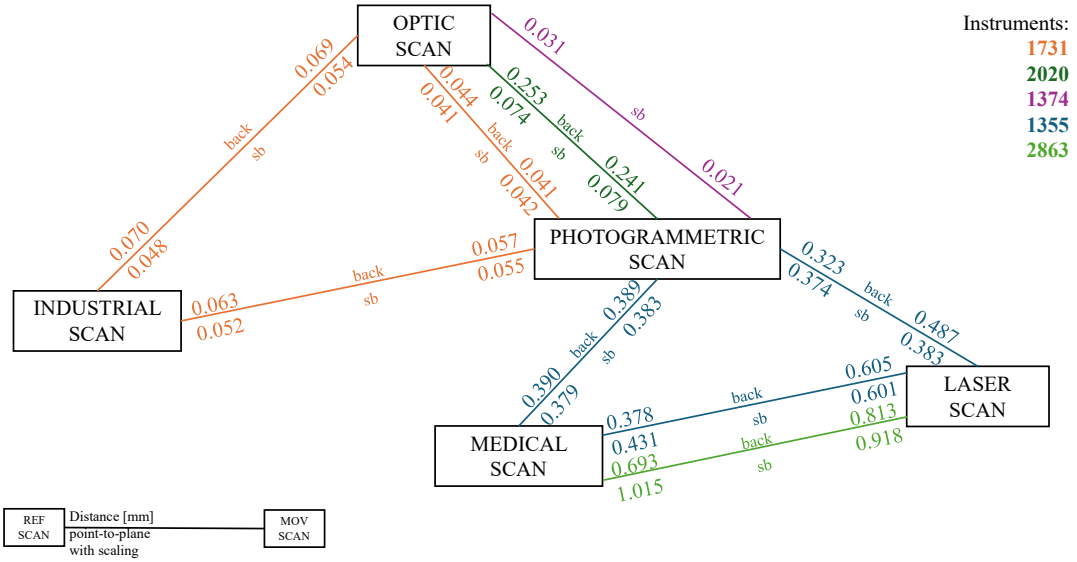

FIG. 7.1 – *Summary of all the mean root squared point to plane distances*

Three instruments have mean root squared distances under the 0.01 mm, the Amati viola 1731, the Borbon cello 1374 and the Amati cello 2020 (only the sound board). The violin Hofmans 1355 and the back of the Amati cello have distances between 0.2 and 0.6

mm. The largest value occur for the Boussu cello 2863 with values up to 1 mm.

Although the exercise is rather simple, it is possible to compute an error to each acquisition technique by using the same formula as previously done to approximate the distance of each comparison as the sum of the error of each technique ($d_{tech_1 tech_2} = e_{tech_1} + e_{tech_2}$). Therefore the mean between all of the comparisons between two methods is calculated and this gives the numbers on figure 7.2

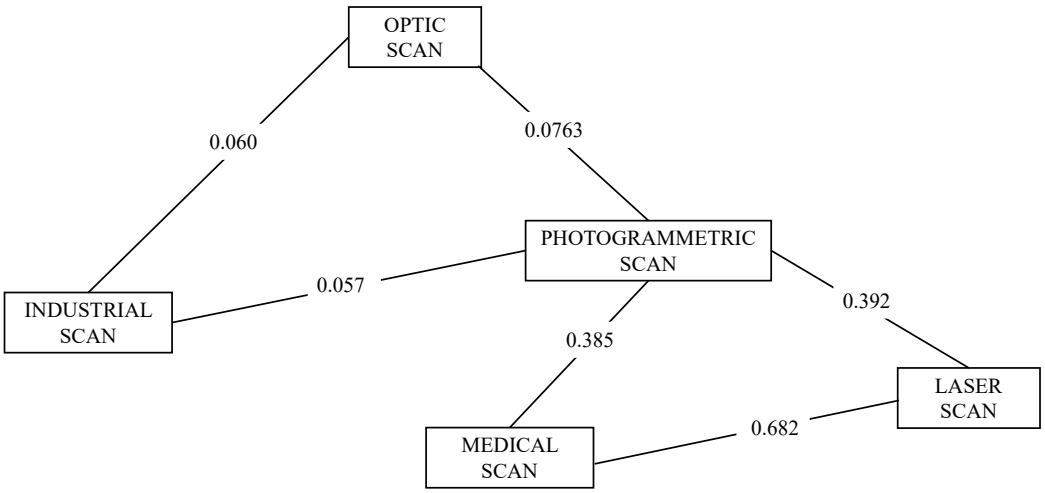

FIG. 7.2 – *Mean distances for each pair (point to plane (mm), full registration with scaling*

The system that needs to be solved is (indu= industrial, opt= optical, phot= photogrammetry, med= medical, las=laser) :

$$\begin{pmatrix} 1 & 1 & 0 & 0 & 0 \\ 1 & 0 & 1 & 0 & 0 \\ 0 & 1 & 1 & 0 & 0 \\ 0 & 0 & 1 & 0 & 1 \\ 0 & 0 & 1 & 1 & 0 \\ 0 & 0 & 0 & 1 & 1 \end{pmatrix} \begin{pmatrix} e_{indu} \\ e_{opt} \\ e_{phot} \\ e_{med} \\ e_{las} \end{pmatrix} = \begin{pmatrix} 0.060 \\ 0.057 \\ 0.076 \\ 0.392 \\ 0.385 \\ 0.682 \end{pmatrix} \tag{7.1}$$

Solving the system with the least squares function of *numpy.linalg*, *lstsq*, the errors are :

- $e_{indu} = 0.0196$
- $e_{opt} = 0.0378$

- $e_{phot} = 0.0421$
- $e_{med} = 0.3463$
- $e_{las} = 0.3393$

There is a clear difference between the first three values, the optic, industrial and photogrammetric scan, all below 0.05 mm, and the last two, the medical and laser scan around 0.3 mm. This is not a surprising result as the comparisons involving the latter are at least five times larger than the ones for the other.

The next figure is a graphical representation of the distances, written in black and the errors computed before are drawn in color (red = optic, blue = industrial, violet = medical, green = laser scan and yellow = photogrammetry). The technologies were separated in the two groups described before to have better scales.

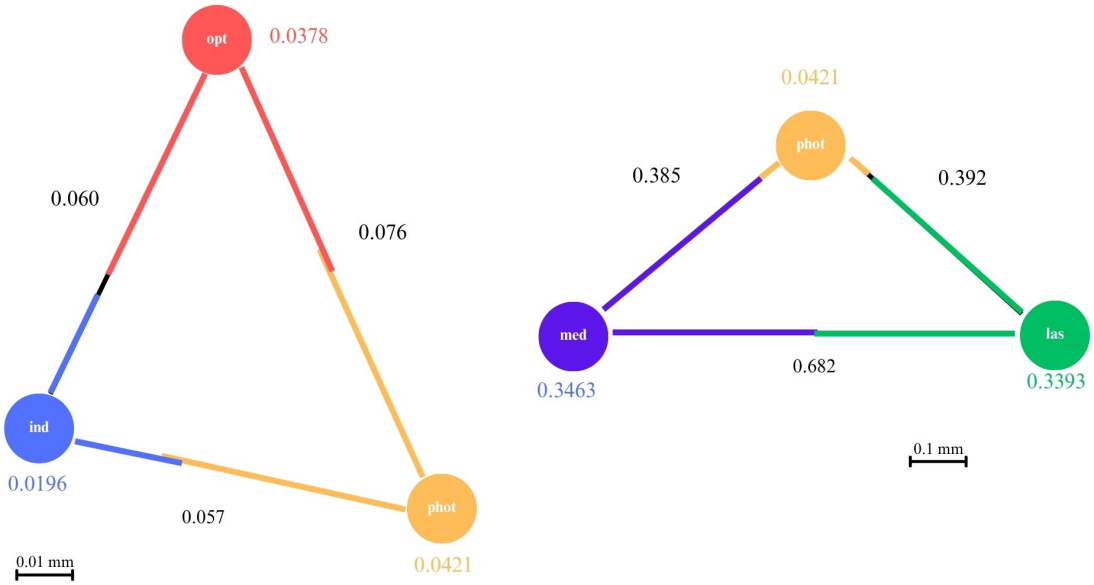

FIG. 7.3 – *Schematic representation of the errors*

From these figure, and the numbers calculated previously, the industrial scan comes as the one contributing the least to the distances. The two other technologies with good results are the optic scan and the photogrammetry. On the other hand, the medical and the laser scan have errors close to 0.35 mm.

It is still to be reminded that these results are dependent on all of the conditions of the experiments and hardly generalizable but the results for the optic scan and the photogrammetry, that are way more easier approaches than the industrial scan, are promising.

Conclusion

This work started by analyzing the different acquisition techniques one could use to scan an object and how these techniques have been carried out in practice. Then the standardization of the output was explained such that the comparisons would be performed on entities with the same shape. A metric and a registration process were established to measure the difference between those meshes. All of this led to the comparisons of the different acquisition techniques for five instruments and a more global analysis.

Three instruments revealed excellent distances with mean values around 0.05 millimeters, the Amati viola 1731, the Amati cello 2020 and the Borbon cello 1374. These three instruments shared the three acquisition techniques that are the photogrammetry, optical scanning, and industrial scanning. For these three methods an estimation of the error was calculated and the industrial scan achieved the smallest error at 0.0196 mm, the optical scan and photogrammetry have values of 0.0378 mm and 0.0421 mm, respectively which are excellent and indicative of high accuracy. The two other technologies that are the medical CT scan and the laser scan have almost the same error that is about 0.34 mm. This is significantly larger than the others but still represents a good result. iPad technologies such as TrueDepth and LiDAR also showed for some of the cases distances with the photogrammetry close to 0.2 mm.

This work, and the results obtained in the very specific conditions detailed, demonstrate that alternatives to more demanding technologies, such as photogrammetry and optical scanning, are reliable and can be used for further analysis with a high precision.

References

[1] Ceulemans, Anne-Emmanuelle ; Glineur, François ; Fisette, Paul ; Beghin, Philémon ; Thys, Iona. Baroque Violas with Reduced Soundboxes: An Evaluation Method. In: The Galpin Society Journal : for the study of musical instruments, Vol. LXXVI, p. 109-126 (2023)

[2] Boyden, David D., Peter Walls, Peter Holman, Karel Moens, Robin Stowell, Anthony Barnett, Matt Glaser, Alyn Shipton, Peter Cooke, Alastair Dick, and Chris Goertzen. "Violin." Grove Music Online. 2001; Accessed 4 Jan. 2025.

[3] Motte L., Conception d'un outil mathematique/informatique pour la classification d'instruments a archet, Master thesis, UCL/EPL, 2017, prom. P. Fisette and A.-E. Ceulemans

[4] Lothaire R., Characterization of violins: a digital tool at the service of organology, Master thesis, UCL/EPL, 2019, prom. P. Fisette, F. Glineur and A.-E. Ceulemans

[5] Beghin P., A digital tool at the service of organology Validation of a photogrammetric approach , Master thesis, UCL/EPL, 2021, prom P. Fisette, F. Glineur and A.-E. Ceulemans

[6] P. Cignoni, M. Callieri, M. Corsini, M. Dellepiane, F. Ganovelli, G. Ranzuglia MeshLab: an Open-Source Mesh Processing Tool Sixth Eurographics Italian Chapter Conference, page 129-136, 2008

[7] P. Beghin, A.-E. Ceulemans, P. Fisette and F. Glineur (2023) Validation of a photogrammetric approach for the objective study of early bowed instruments. Heritage Science

[8] Glira, P., Pfeifer N., Briese, C., & Ressl, C. A correspondence framework for ALS strip adjustments based on variants of the ICP algorithm. Photogrammetrie - Fernerkundung - Geoinformation. 2015; 2015(4), 275-289

[9] Michael Garland and Paul S. Heckbert. 1997. Surface simplification using quadric error metrics. In Proceedings of the 24th annual conference on Computer graphics and interactive techniques (SIGGRAPH '97). ACM Press/Addison-Wesley Publishing Co., USA, 209–216. https://doi.org/10.1145/258734.258849

UNIVERSITÉ CATHOLIQUE DE LOUVAIN
École polytechnique de Louvain
Rue Archimède, 1 bte L6.11.01, 1348 Louvain-la-Neuve, Belgique | **www.uclouvain.be/epl**